Proceedings of ERAD 2006

Modeling mesoscale pattern of mid-latitude convective raincells using weather radar measurements

Mario Montopoli[1,2], Frank Marzano[1,3] Anna Fornasiero[4], and Pier Paolo Alberoni[4]

[1] CETEMPS, L'Aquila, (Italy).

[2] DIEL, University of L'Aquila, (Italy).

[3] DIE, University of Rome La Sapienza, Rome, (Italy).

[4] SIM-ARPA, Bologna, Italy.

1 Introduction

The knowledge of the statistical characteristics of the rain structures is very important in many fields going from hydrology to telecommunication (TLC) applications. For hydrological purposes, the study of convective rain systems is usually finalized to the flood forecasting of river catchments and to the nowcasting of the evolution of extreme precipitation to support civil protection activities (Capsoni and D'Amico, 2004). For TLC applications, new high-frequency terrestrial and satellite systems (e.g., from Ka band to V band), can be strongly affected in their performances by the presence of a raincell or a cluster of cells so their experimental characterization can enhance the channel design (Feral et al. 2000).

Apart from the specific purpose, there is a need to quantitatively characterize the spatial patterns of mesoscale convective systems. Mesoscale convective systems can often present themselves as a single cell or a cell cluster with multiple rain-rate peaks. The goal of this work is to extract useful information from these rainy structures and utilize them to drive the raincell pattern modeling procedure in order to carry out a comparison between the analyzed raincell models each other. From radar measurements several features have been derived such as rain rate peak, average, and root mean square value together with raicell area, gradient average and deviation.

From a raincell pattern modeling point of view, we have investigated several analytical models like EXCELL based on an exponential profile (e.g., Capsoni et al., 1987), GAUCELL based on a Gaussian profile (e.g., Von Hardenberg et al., 2003), HYCELL based on a combination of GAUCELL and EXCELL (Feral et al., 2003) and a new one, here examined named DEXCELL which is based on a combination of two exponential shapes. A crucial aspect of the radar data best-fitting analysis is the assumption, implicitly made by many authors, to consider the modeled rainrate peak as directly comparable to the radar measured one. Indeed, the radar-measured rainrate peak is the measured value of rain rate averaged on degraded radar resolution volume.

Therefore, a correct analysis should first carry out a pixel numerical spatial integration of the raincell analytical models before comparing the modeled observables with radar-measured ones. This paper approaches most basic issues raised above in order to retrieve, model and compare raincell patterns.

Correspondence to: Mario Montopoli.

mmontop@ing.univaq.it

2 Radar Measurements

The rainfall data used in this study have been provided by the C-band operational Doppler radar of S. Pietro Capo fiume (SPC) near Bologna, located in the Po river valley in northem Italy (Alberoni et al., 2001). This dual-polarization radar is placed on a tower with a Cassegrain parabolic antenna without radome, providing a half-power beam-width of 1.0° and a directivity of about 45-dB. The klystron peak-power is 250 kW at 5.6 GHz and the receiver sensitivity is equal to 113 dBm. Procedures to correct for gas absorption, to remove ground-clutter echoes and to identify anomalous propagation conditions are routinely applied. Side-lobe effects at very short ranges (less than 20 km) for low elevations are avoided by choosing higher elevations not affected by this effect.

2.1 Radar data

Four years of radar data, acquired from January 1996 to December 1999 in an operational mode, have been

considered in the present study. We have used only the measured radar reflectivity at horizontal polarization in polar coordinates, here indicated by Z_m. Hereafter the subscript m indicates the radar measured quantity. The radial resolution and the maximum range have been set, respectively, to 250 m and 125 km. Due to orography blockage in the south-western sector of observation, at each bin location we have extracted the value of Z_m relative to the lowest available elevation using a radar visibility map.

The resulting polar map of the measured lowest-bin has been then converted in a picture on a Cartesian regular grid with dimensions of 256x256-km^2 and with spatial resolution of 1km. For easy representation and interpretation, each value $Z_m(i,j)$ at the pixel (i,j) on the Cartesian grid has been converted to surface rainrate $R_m(i,j)$, using a standard power law Z-R relation: $R_m(i,j)=a\cdot[Z_m(i,j)]^b$ with the coefficients a and b equal to those of Marshall-Palmer *(i.e., a=200, b=1.6* with R_m in mm/h and Z_m in mm^{6}m^{-3}). As a result, the measured dataset has been converted into a temporal series of 1558 rainrate maps R_m (or frames) of 256x256 pixels.

2.2 Raincell recognition algorithm

The raincell recognition step is crucial for a further analysis between measured and modeled rain patterns. By means of this new identification algorithm, we have extracted 20560 raincells from the 1558 measured rainfall Cartesian maps. The raincell identification process is founded by the main following steps repeated for each rainrate map:

(a) all the Cartesian coordinates of the local intensity maxima are identified. A local maximum is defined as a pixel that is larger than both its 8-connected neighbor-pixel values and the threshold of 10 mm/h, and it is defines the measured raincell peak or maximum R_{Mm}. In order to privilege the highest values of raincell peaks, a sorting procedure of the local maxima within the rain map $R_m(i,j)$, in a decreasing order, is made. Therefore, all the local maxima are visited beginning from the highest value.

(b) On each R_{Mm} location, the rain intensities inside a pixel spatial box $R_{mb}(i,j)$ of size *25x25 km* are considered. The procedure continues computing the bi-dimensional (2D) autocorrelation function $C_{Rmb}(l_s)$ of $R_b(i,j)$ with l_s the spatial 1-km lag counter, a function strictly linked to the local spatial texture of rain field in a surrounding area of R_{Mm}.

(c) The average rainrate intensity on the isoline of $C_{Rmb}(k)$ at the level where the $C_{Rmb}(k)$ maximum is reduced of about 36% is taken as the raincell threshold R_{Tl}. Lastly, around R_{Mm} all the 8-connected values are explored ascribing the pixels larger than R_{Tl}, and smaller than R_{Mm} to the measured raincell field denoted as $R_{mc}(i,j)$. In order to avoid the effect of noise on small rainy structures, the threshold R_{Tl} is automatically set to 5 mm/h if this value is overtaken negatively (Von Hardenberg et al., 2003).

2.3 Description of main raincell features.

By means of the recognition algorithm introduced in the previous section two types of rain structures have been identified: the single-peak (SP) and multi-peak (MP) raincells. The SP raincells are structures whose values are distributed around a single local dominant peak value R_{Mm} and where the rain intensity decreases with the distance within the raincell area. Since it can happen that more than a one local maximum exists inside a SP raincell area, we have classified as SP raincells all the rainy structures where the local maxima values do not overcome the threshold of the 30% of R_{Mm} From the previous analysis a set of 2800 SP and 8190 MP raincells has been finally extracted.

In this section a very short and partial description of the spatial characteristics of the rain field inside each SP and MP raincell is discussed. Fig. 1 gives a comprehensive picture of the *morphology* of the raincell measured observables such as the rain cell area A_{Rm}, the raincell peak R_{Mm}, the average raincell field R_{Am}, the raincell root mean square value R_{Sm}, the raincell gradient average G_{Am} and the gradient root mean square value G_{Sm}.

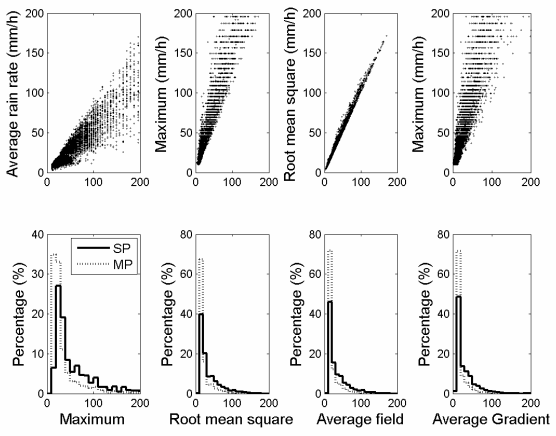

Fig. 1. Scatter and relative bar plots of raincell observables. In the lower panel the dotted bars are referred to multi-peak raincells whereas the solid lines are referred to the single-peak raincells.

The upper panels of Fig. 1 shows the scatter plots of some rain cell parameters, previously mentioned, whereas the lower panels of the same figure shows the probability density distribution of the same parameters.

The analysis of average and median values of the raincell observables point out that R_{Mm}, R_{Am}, R_{Sm}, G_{Am} of the SP raincells are distribuited on larger average values with respect to the MP raincells. This means that SP raincells are on average more intense than MP cells. In the next section we compare these raincell features with the same quantities synthesized by the the raincell models.

3 Raincell models

The aim of a raincell analytical model is to describe the rain rate horizontal distribution. We can formulate the problem of raincell modeling considering: (a) a decaying unimodal function of the rain intensities around its peak (or unimodal models), (b) a combination of two functions so that the rain cell core and the surrounding intensities are differently described (or hybrid models). The general

analytical definition of the hybrid pattern model has the following expression:

$$R_p(x,y)=\begin{cases} R_{Mp}\cdot\exp\left[-\left(\dfrac{x^2}{a_p^2}+\dfrac{y^2}{b_p^2}\right)^{\frac{1}{k}}\right] & if\ R_p \geq R_{Th} \\ R_{Msp}\cdot\exp\left[-\left(\dfrac{x^2}{a_{sp}^2}+\dfrac{y^2}{b_{sp}^2}\right)^{\frac{1}{k_s}}\right] & if\ R_{Tl} \leq R_p < R_{Th} \end{cases} \quad (1)$$

where $R_p(x,y)$ is the value of rain rate pattern at the Cartesian position (x,y) of a synthetic raincell with the peak R_{Mp} in (0,0), the couple (a_p, b_p) the distances from the peak along the x and y axes respectively at the rain rate value equal to $e^{-1}\cdot R_{Mp}$, the value R_{Th} is the separation threshold between the central and the surrounding portion, labeled with the subscript "*s*" of the hybrid pattern model. In our context the integers k and k_s can be 1 or 2 specifying a Gaussian or exponential horizontal profile, respectively, whereas the subscript p labels the type of examined raincell model. Eq. (1) is quite general: when $R_{Th}=R_{Tl}$, it describes a single unimodal function (i.e. the surrounding portion of R_p vanishes). For example, a synthetic raincell with Gaussian rain horizontal profile, named as GAUCELL, corresponds to the choice of k=1, p=g and $R_{Th}=R_{Tl}$, whereas k=2, p=e and $R_{Th}=R_{Tl}$ pertains to an exponential shaped raincell, named as EXCELL.

Once we fix the values of k, these unimodal models are described by means of three parameters R_{Mp}, a_p, b_p. When $R_{Th}\neq R_{Tl}$, the hybrid model is described and for k=1, k_s=2 and p=h, we obtain the HYCELL model, whereas for k=2, k_s=2 and p=d we obtain the new model introduced in this work, named DEXCELL. Once we fix the values of k and k_s, the hybrid model is identified by means of the pattern parameter vector whose components are: R_{Mp}, a_p, b_p, R_{Msp}, a_{sp}, b_{sp} and R_{Th}. It is worth noting that, when we examine a hybrid model, we have to consider two supplementary equations in order to guarantee the continuity condition at the separation interface, defined by the threshold R_{Th}, between the core and the surrounding portion of the synthesized raincell. In order to carry out a meaningful comparison between the measured and modeled-pattern quantities, we should take account that the measured raincell intensity $R_{mc}(i,j)$ is the value of rain rate averaged over the area of the Cartesian pixel (i,j). For example the raincell peak value R_{Mm} is representative of a region equal to the square of the horizontal spatial resolution of the analyzed map (1 km^2 in our case), whereas the analytical curves are referred to the peak value R_{Mp} of (1). From this consideration, we can argue that the measured and modeled-pattern raincell observables values are not directly comparable. In order to remove this ambiguity, we have performed a numerical integration of the synthesized raincell, given in eq. (1) as follows:

$$R_p(i,j)=\frac{1}{\Delta x\Delta y}\cdot\int_{j-\frac{\Delta x}{2}}^{j+\frac{\Delta x}{2}}\int_{i-\frac{\Delta y}{2}}^{i+\frac{\Delta y}{2}}R_p(x,y)\cdot dx\,dy \quad (2)$$

where $R_p(i,j)$ is the value of rain rate representative of the pixel i,j of a synthetic raincell, and $\Delta x=\Delta y$ are the horizontal spatial resolutions along the x and y directions respectively but in this case is $\Delta x=\Delta y$=1 km. If we consider $R_p(i,j)$, instead of $R_p(x,y)$, we can compute the modeled raincell observables by means of the same methodology utilized for the measured ones.

4 Results

For all the SP and MP raincells, extracted from the C-band radar maps, the pattern parameter vector defining the integrated models EXCELL, GAUCELL, HYCELL and DEXCELL have been computed according to the minimization process of an error criterium (or distance) between the measured and model-pattern observable features.

Once the model parameters are retrieved for each raincell model setup, the performance indicators, such as the the average error m_ε, root mean square error (RMSE) value s_ε, and the error correlation coefficient ρ_ε between the measured and the synthesized raincell features were computed. Figs. 2 and 3 summarize the indicators of the raincell performances for each observable separately, for the 4 integrated raincell models here considered and for the SP and MP raincells, respectively.

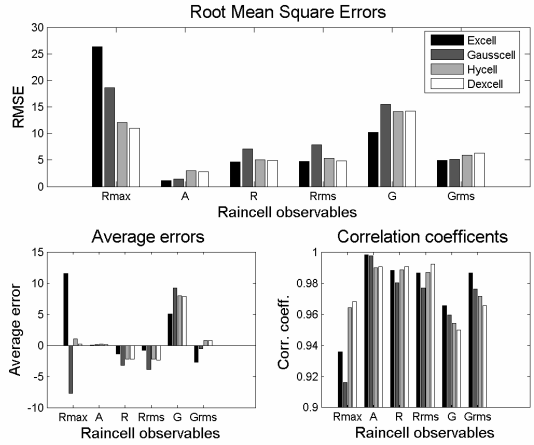

Fig. 2. Performances of the integrated SP raincell model. On the top panel, the root mean square errors of the synthesized raincell observables. On the lower left panel, the average errors of the synthesized raincell observables. On the lower right panel the correlation coefficient of the synthesized rain cell observables.

These plots give an overall view about the performances of the raincell models underlining the raincell characteristics more difficult to reproduce. Raincell maximum and gradient give the major contribute to the differences between the measured and modeled features. Fig. 2 and 3 show, on the lower left panels, for both the typology of raincell, that the average error of the raincell maximum is negative for GAUCELL and positive for the other models. Indeed, for EXCELL we observe a significant average overestimate of the peak value (m_ε=11.70 for SP and m_ε =10.14 for MP) as opposed to the GAUCELL (m_ε =-5.97 for SP and m_ε =-2.26

for MP), HYCELL (m_ε =5.58 for SP and m_ε =4.79 for MP) and DEXCELL (m_ε =4.44 for SP and m_ε =3.89 for MP).

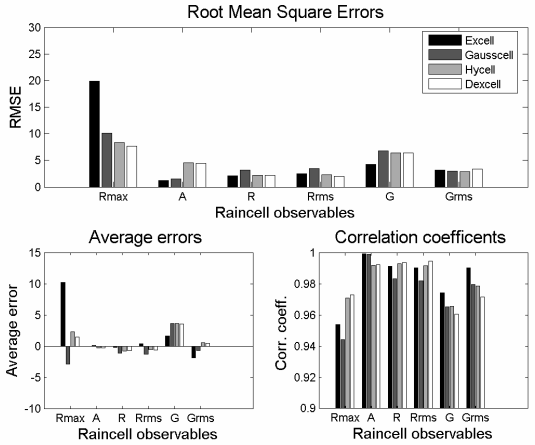

Fig. 3. Performances of the integrated MP raincell model. On the top panel, the root mean square errors of the synthesized raincell observables. On the lower left panel, the average errors of the synthesized raincell observables. On the lower right panel the correlation coefficient of the synthesized rain cell observables.

The upper panel of Fig. 2 and 3 shows that the RMSE value relative to the raincell maximum due to the EXELL model is larger than the other ones, whereas for GAUCELL there is a considerable variation of the RMSE value relative to its maximum from 18.62 for SP to 10.10 for MP raincells. This leads to the consideration that GAUCELL can have a better capability to model the raincell maximum of the MP raincells than SP patterns. The lower right panel of Fig. 2 and 3 show high values of the correlation coefficient for all the raincell features and raincell models.

In order to compare the performance of the analyzed raincell models for both SP and MP raincells typology, the total RMSE has been computed. Total RMSE is defined as the square root of the summation, through the raincell features, of RMSE of each raincell. The computed values of total RMSE are 20.91 for EXCELL, 13.45 for GAUCELL, 12.17 for HYCELL and 11.84 for DEXCELL. Nevertheless the impact of the integration process on the synthesized raincell peak the value of total RMSE for EXCELL model is larger than the others ones. Eventually, we can appreciate the better accuracy of the hybrid models to reproduce the overall characteristics of the raincells as opposed to their major complexity. On the other hand the unimodal models show higher errors to reproduce the rain cell maximum and this aspect tend to degrade their overall performances.

5 Conclusions

A spatial characterization of mid-latitude mesoscale rain fields from C-band radar measurements has been performed by means of a systematic analysis and modeling of convective raincell 2D shapes. A new accurate algorithm for raincell identification has been introduced and briefly discussed. From this analysis, a quality-controlled set of 10990 raincells has been extracted and a partition of this set has been made in order to distinguish from single-peak and multi-peaked raincells. Some raincell features have been showen for both the single-peaked and multi-peaked raincells and their several differences have been pointed out. Four two-dimensional analytical models of rainfall horizontal pattern, such as the exponential (EXCELL), Gaussian (GAUCELL) and hybrid (HYCELL), have been reviewed jointly together with a new model named DEXCELL. Considering that a measured raincell intensity is the value representative of rain rate averaged over the areal pixel, we have performed a numerical integration of the synthesized raincell equations in order to carry out a meaningful comparison between the measured and modeled raincell.

The statistical results of this comparison have highlighted that the hybrid models are more accurate with respect to the unimodal ones, event though this better performance is at expenses of a higher mathematical complexity. No appreciable differences have found between the HYCELL and DEXCELL. This might be interpreted underlining that hybrid model accuracy is less dependent from the utilized shape to describe the convective rainrate core portion of the raincell and more sensitive to the way to model the surrounding portion of the raincell. Finally, it should be noted that the EXCELL model tends to provide unrealistic values of rainrate maximum, especially when the average raincell field of the extracted raincell is large. On the contrary, the GAUCELL model tends to underestimate the central portion of the raincells and shows a total RMSE lower than EXCELL.

Acknowledgements: This work has been partially supported by the Civil Protection Directorate of Region Abruzzo.

References

Alberoni, P.P., T. Andersson, P. Mezzasalma, D.B. Michelson, and S. Nanni, 2001: Use of the vertical reflectivity profile for identification of anomalous propagation. *Meteorol. Appl.*, **8**, 257-266.

Capsoni, C. and M. D'Amico, 2004: Morphological description of the rain structures in the Padana valley. *Proc. of ERAD04.*, 15-64.

Von Hardenberg, J., L. Ferraris, and A. Provenzale, 2003: The shape of convective rain cells. *Geophysical Research Letters*., 10.1029/2003GL018539.

Féral, L., F. Mesnard, H. Sauvageot, L. Castanet, and J. Lemorton, 2000: Rain Cell Shape and Orientation Distribution in South-West France., *Phys. Chem*. Earth B, **25**, 1073-1078.

Féral, L., H. Sauvageot, L. Castanet, and J. Lemorton, 2003: A new hybrid model of the rain horizontal distribution for propagation studies: 1. Modeling of the rain cell. *Radio Science*., 10.1029/2002RS002802.